

Superconductivity in Ternary Scandium Tellurides with 3*d*, 4*d*, and 5*d* Transition Metals

Yusaku Shinoda¹, Yoshihiko Okamoto^{2*}, Youichi Yamakawa³, Haruka Matsumoto², Daigorou Hirai¹, Koshi Takenaka¹

¹*Department of Applied Physics, Nagoya University, Nagoya 464-8603, Japan*

²*Institute for Solid State Physics, University of Tokyo, Kashiwa 277-8581, Japan*

³*Department of Physics, Nagoya University, Nagoya 464-8602, Japan*

Some *d*-electron superconductors, such as cuprates and iron arsenides¹⁻⁸, exhibit various unique superconductivities that have attracted attention in condensed matter physics. However, they are not ubiquitous. Exotic superconductivity in *d*-electron systems usually appears in materials with specific combinations of transition-metal elements and crystal structure, which precludes a full understanding thereof. Here we report the discovery of bulk superconductivity in Sc₆MTe₂ with seven kinds of transition-metal elements M. The critical temperatures for M = 3*d* were higher than those for M = 4*d* and 5*d* and varied systematically, reaching the highest $T_c = 4.7$ K for M = Fe. The upper critical fields for M = Os and Ir were significantly enhanced by the strong spin-orbit coupling. These results showed Sc₆MTe₂ to constitute a unique family of *d*-electron superconductors displaying superconductivity in all 3*d*, 4*d*, and 5*d* cases, in which the electron correlation and spin-orbit coupling of *d* electrons played roles.

Superconductivity in *d*-electron systems has been one of the central issues in condensed matter physics. There are many outstanding superconductors, such as cuprates¹, iron arsenides and selenides^{2,3}, spinel LiTi₂O₄⁴, layered perovskite Sr₂RuO₄⁵, hydrate Na_xCoO₂·*n*H₂O⁶, β-pyrochlore KO₂O₆⁷, and kagome CsV₃Sb₅⁸. The *d* electrons of the transition metals play a major role in determining their electrical properties and the cooperation between various features of *d* electrons, such as strong electron correlation, strong spin-orbit coupling, and strong spin and orbital fluctuations, results in the emergence of unique unconventional superconductivities. However, such *d*-electron superconductivities appear only in materials with specific combinations of transition metal elements and crystal structure. For example, almost all transition metal compounds that are isostructural to the above superconductors but contain other transition metal elements do not exhibit superconductivity. A recently discovered layered nickelate superconductor, which is a Ni analogue of high- T_c cuprates, is a rare counter-example⁹. This nature of *d*-electron superconductors prevents a complete understanding of their features based on systematic experimental studies.

We report herein the ternary telluride series Sc₆MTe₂ as a unique family of *d*-electron superconductors incorporating 3*d*, 4*d*, and 5*d* electron systems. All of the Sc₆MTe₂ compounds described in this letter crystallized in the hexagonal Zr₆CoAl₂-

type structure with space group $P\bar{6}2m$ without inversion symmetry, as shown in Fig. 1(a). This crystal structure is one of the ordered Fe₂P-types, in which the P sites are regularly occupied by M and Te atoms in a 1:2 ratio. As shown in the right-handed panel of Fig. 1(a), the M atoms form one-dimensional chains along the *c*-axis. In terms of superconductivity, transition metal compounds with ZrNiAl-type structure, which is another ordered Fe₂P-type in which the Fe sites are regularly occupied by two kinds of metal atoms in a 1:1 ratio, have been studied as 4*d*- and 5*d*-electron superconductors represented by ZrRuP¹⁰⁻¹³. However, to the best of our knowledge, no Zr₆CoAl₂-type superconductor has hitherto been reported. Sc₆MTe₂ with M = Mn, Fe, Co, Ni, Ru, Rh, Os, and Ir has been reported to crystallize in a Zr₆CoAl₂-type structure, but the physical properties of these systems have not been reported thus far^{14,15}. We have now measured the physical properties of synthesized Sc₆MTe₂ polycrystalline samples with the above M elements and found bulk superconductivity in all samples except for that with M = Mn. The highest transition temperature was found to be $T_c = 4.7$ K in Sc₆FeTe₂. The T_c values for compounds with M = 3*d* elements proved to be higher than those for compounds with M = 4*d* and 5*d* elements and showed systematic variation according to atomic number. The upper critical fields for compounds with M = 5*d* elements are higher than those for M = 3*d* relative to their T_c , most likely reflecting the chemical

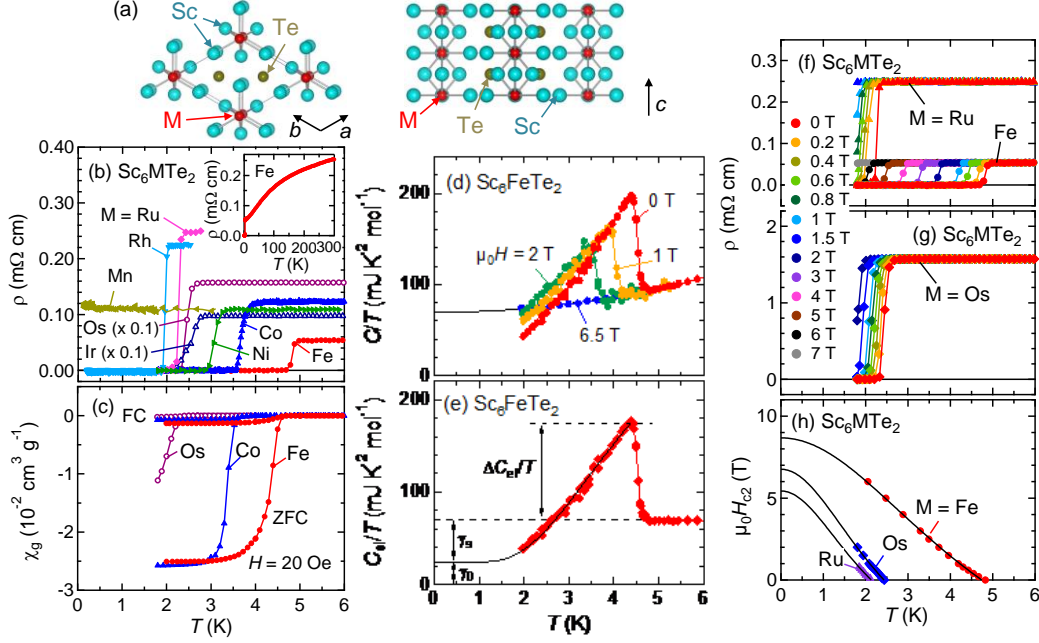


Figure 1. Crystal structure and superconducting properties of Sc_6MTe_2 polycrystalline samples. (a) Crystal structure of Sc_6MTe_2 drawn using VESTA¹⁶. (b) Temperature dependence of electrical resistivity. The inset shows the Sc_6FeTe_2 data at high temperatures. (c) Temperature dependence of field-cooled (FC) and zero-field cooled (ZFC) magnetic susceptibility measured at a magnetic field of 20 Oe. (d) Temperature dependence of heat capacity divided by temperature, C/T , of Sc_6FeTe_2 measured at various magnetic fields from 0 to 6.5 T. The solid curve shows a fit to the equation $C/T = AT^2 + \gamma$ of the 1.9–4.5 K data taken at $m_0H = 6.5$ T, yielding $A = 1.07(3)$ $\text{mJ K}^{-4} \text{mol}^{-1}$ and $\gamma = 69.3(3)$ $\text{mJ K}^{-2} \text{mol}^{-1}$. (e) Temperature dependence of the electron heat capacity divided by temperature, C_e/T , for Sc_6FeTe_2 obtained by subtracting the lattice contribution from the data shown in (d). The broken line shows the electron heat capacity in the normal state γ . The solid curve shows a fit using the α model. (f, g) Temperature dependences of electrical resistivity of $M = \text{Fe, Ru, and Os}$ measured at various magnetic fields. (h) Temperature dependence of the upper critical field $H_{c2}(T)$ for $M = \text{Fe, Ru, and Os}$ determined from the midpoint of the drop in the resistivity data. The solid curves show a fit to the GL formula.

trend of the spin-orbit coupling of d -electrons in M atoms.

The temperature dependence of electrical resistivity, ρ , of a Sc_6FeTe_2 polycrystalline sample is shown in Fig. 1(b). As shown in the inset, Sc_6FeTe_2 showed metallic ρ , decreasing on lowering the temperature. When the temperature was further decreased, ρ showed a sharp drop to zero between 5.0 and 4.7 K. As shown in Fig. 1(c), the zero-field-cooled (ZFC) and field-cooled (FC) magnetization data showed strong diamagnetic signals below 4.7 K, indicating that a bulk superconducting transition occurred at this temperature. The shielding fraction at 1.8 K was estimated to be high, at 150%, considerably larger than 100%, probably due to a demagnetization effect. The jump observed in the heat capacity data shown in Fig. 1(d) also supported the emergence of bulk superconductivity. Taking the zero-resistivity temperature, the onset of the magnetization drop, and the midpoint of the heat capacity jump to be 4.7, 4.7, and 4.6 K, respectively, the T_c was determined as 4.7 K.

Bulk superconducting transitions also appeared in the other Sc_6MTe_2 polycrystalline samples, except for $M = \text{Mn}$. Their ρ data showed zero resistivity, as shown in Fig. 1(b). Corresponding to these superconducting transitions, large diamagnetic signals and jumps in heat capacity appeared in

Table 1. T_c and $H_{c2}(0)$ of Sc_6MTe_2 . The T_c values were determined by the zero-resistivity temperature, the onset of the magnetization drop, and the midpoint of the heat capacity jump. The $H_{c2}(0)$ values were determined by fitting the midpoint of the resistivity drop to the GL formula.

$3d$ element	Mn	Fe	Co	Ni
T_c (K)	< 0.1	4.7	3.5	2.7
$\mu_0 H_{c2}(0)$ (T)		8.8	6.2	3.7
$4d$ element		Ru	Rh	
T_c (K)		1.9	1.9	
$\mu_0 H_{c2}(0)$ (T)		5.4	3.5	
$5d$ element		Os	Ir	
T_c (K)		2.2	2.0	
$\mu_0 H_{c2}(0)$ (T)		6.8	7.3	

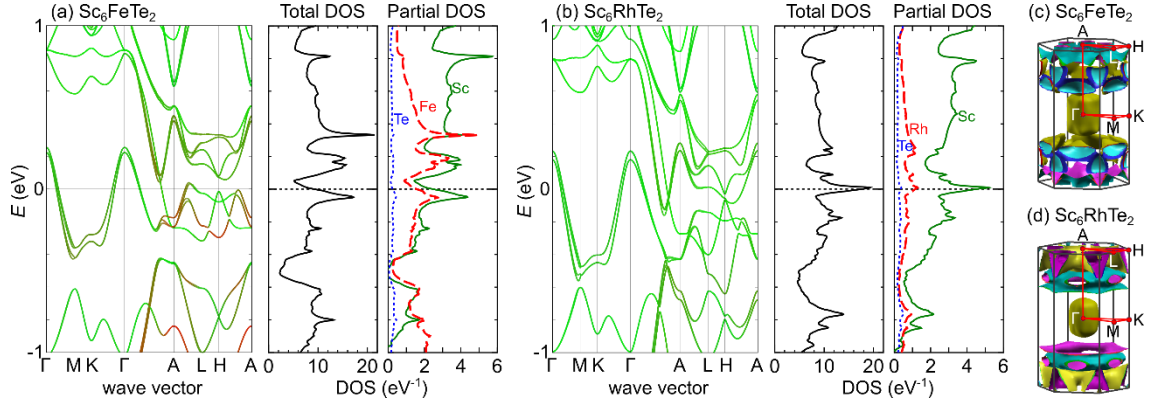


Figure 2. The electronic states of Sc_6FeTe_2 and Sc_6RhTe_2 with spin-orbit coupling. (a) and (b) show the electronic structures (left) and DOS (right) of Sc_6FeTe_2 and Sc_6RhTe_2 , respectively. The Fermi level is set to 0 eV. (c) and (d) show the Fermi surfaces of Sc_6FeTe_2 and Sc_6RhTe_2 , respectively.

the magnetization and heat capacity data, as shown in Fig. 1(c) and Supplementary Fig. 2(a, b), respectively, indicating the emergence of bulk superconductivity. As shown in Table I, seven compounds, except for Sc_6MnTe_2 , exhibited a bulk superconducting transition above 1.8 K. Sc_6MnTe_2 did not show superconductivity above 0.1 K.

The T_c values of Sc_6MTe_2 showed characteristic M dependences. Four compounds with $M = 4d$ and $5d$ elements displayed almost the same T_c of approximately 2 K, as shown in Table I, but those with $M = 3d$ elements displayed higher values and exhibited systematic variation with atomic number. Sc_6NiTe_2 showed $T_c = 2.7$ K, which increased with decreasing atomic number, and Sc_6FeTe_2 showed the highest T_c of 4.7 K. In the following, we discuss the role of M atoms in the chemical trend of T_c in Sc_6MTe_2 . First-principles calculations showed that the $3d$ orbitals of M atoms make a large contribution to the electronic states near the Fermi energy, E_F . As shown in Fig. 2(a), E_F of Sc_6FeTe_2 is located just above the peak of the density of states, $D(E)$, and the contributions from Fe and Sc, which mainly involve their $3d$ orbitals, are dominant for $D(E_F)$. A similar tendency was seen for compounds with other $3d$ elements. In contrast, the E_F of Sc_6RhTe_2 is located at the top of $D(E)$, as shown in Fig. 2(b), but mainly Sc contributes to the electronic state at E_F and the contribution from Rh is small. In other $4d$ and $5d$ cases, the contribution of M atoms at E_F is also small.

As shown in Fig. 2(c, d), Sc_6MTe_2 has two kinds of Fermi surfaces. Firstly, there are spherical hole surfaces surrounding the Γ point, which are slightly elongated along the k_z direction. Secondly, there are complex-shaped surfaces, mainly existing at $\pi/c > |k_z| > \pi/2c$ of the Brillouin zone. The former surfaces mainly consist of Sc $3d$ orbitals and have almost the same shape for all of the studied M. In contrast, the latter surfaces have a considerable contribution from M $3d$ orbitals, in addition to the Sc $3d$ orbitals, in the $M = 3d$ cases, different from $M = 4d$ and $5d$ cases, in which contributions from the M $4d/5d$ orbitals are small. The very similar T_c values for $M =$

$4d$ and $5d$ elements suggest that the superconductivity at approximately 2 K appears when the Sc $3d$ electrons dominantly contribute to the electronic state at E_F . In contrast, the higher and element-dependent T_c for $M = 3d$ elements indicates that the latter Fermi surfaces with a significant contribution from the M $3d$ orbitals contribute to the emergence of superconductivity.

The question then arises as to how the $3d$ electrons of M atoms contribute to the superconductivity in Sc_6MTe_2 . The $D(E_F) = 17.9 \text{ eV}^{-1}$ for Sc_6RhTe_2 ($T_c = 1.9$ K) is almost twofold larger than 9.3 eV^{-1} for Sc_6FeTe_2 ($T_c = 4.7$ K), as shown in Fig. 2(a, b), reflecting the fact that the E_F in Sc_6RhTe_2 is located at the peak of $D(E)$, whereas that in Sc_6FeTe_2 is not. The Sommerfeld coefficients calculated from these $D(E_F)$ values are $\gamma_{\text{band}} = 42$ and $22 \text{ mJ K}^{-2} \text{ mol}^{-1}$ for Rh and Fe, respectively. In the case of Rh, the experimentally determined Sommerfeld coefficient is $\gamma = 43 \text{ mJ K}^{-2} \text{ mol}^{-1}$, which is almost identical to γ_{band} . In contrast, $\gamma = 69 \text{ mJ K}^{-2} \text{ mol}^{-1}$ for Sc_6FeTe_2 is more than three times larger than γ_{band} , suggesting that the γ of Sc_6FeTe_2 is significantly enhanced by strong electron correlation and/or electron-phonon interaction of the Fe $3d$ electrons. As shown in Fig. 1(e), the electron heat capacity divided by temperature, C_{el}/T , for $M = \text{Fe}$ exhibited a large jump associated with the superconducting transition. The C_{el}/T data could be well fitted by using the sum of superconducting contribution according to the α model and the constant γ_0 , i.e., residual γ , yielding $\gamma_0 = 24 \text{ mJ K}^{-2} \text{ mol}^{-1}$. The magnitude of the jump at T_c was estimated to be $\Delta C_{el}/(\gamma - \gamma_0)T_c = 2.4$ using $\Delta C_{el}/T_c = 110 \text{ mJ K}^{-2} \text{ mol}^{-1}$ and $\gamma - \gamma_0 = 45 \text{ mJ K}^{-2} \text{ mol}^{-1}$, which greatly exceeds the weak-coupling limit of 1.43 for conventional Bardeen-Cooper-Schrieffer (BCS) superconductivity. There is ambiguity in the estimation of γ_0 , but even assuming $\gamma_0 = 0$, $\Delta C_{el}/(\gamma - \gamma_0)T_c$ is still larger than 1.43, indicating that Sc_6FeTe_2 exhibits strong-coupling superconductivity with strong attracting interactions in Cooper pairs. It would be interesting if the spin and orbital fluctuations of $3d$ electrons in Fe atoms, which form one-

dimensional chains as shown in Fig. 1(a), were to contribute to the emergence of this strong-coupling superconductivity. In fact, in the case of $M = \text{Mn}$, next to Fe in the periodic table, superconductivity was not observed above 0.1 K. As shown in Supplementary Fig. 3, the magnetic susceptibility of Sc_6MnTe_2 strongly increases below 50 K, unlike that of Sc_6CoTe_2 , showing Pauli paramagnetic behavior. It is most likely that Cooper pair formation is inhibited by the strong magnetism of Mn $3d$ electrons.

The upper critical field $H_{c2}(T)$ also strongly depends on the M elements in Sc_6MTe_2 . Figures 1(f, g, h) show the r of Sc_6MTe_2 with group 8 elements measured at various magnetic fields and $H_{c2}(T)$ determined from the midpoint of the resistivity drop at each magnetic field, respectively. The H_{c2} data were fitted to the Ginzburg-Landau (GL) formula $H_{c2}(T) = H_{c2}(0)[1 - (T/T_c)^2]/[1 + (T/T_c)^2]$, yielding $\mu_0 H_{c2}(0) = 8.77(8)$, $5.43(2)$, and $6.76(9)$ T and GL coherence length $\xi_{\text{GL}} = 6.2$, 7.8 , and 7.0 nm for $M = \text{Fe}$, Ru , and Os , respectively. As can be seen from the slopes of the fitting curves in Fig. 1(h), the ratio of $H_{c2}(0)$ to T_c increases in the order of Fe, Ru, and Os. Thus, $\mu_0 H_{c2}(0) = 6.76$ T for $M = \text{Os}$ considerably exceeds the Pauli limit determined by paramagnetic effects in the singlet superconducting state, $\mu_0 H_{c2}(0)/T = 1.84T_c/\text{K} = 4.5^{17}$, although $H_{c2}(0)$ for $M = \text{Fe}$ is lower than the Pauli limit value. As shown in Table I and Supplementary Fig. 4, $\mu_0 H_{c2}(0) = 7.3$ T for $M = \text{Ir}$ also exceeded the Pauli limit of 4.7 T, suggesting that these high $H_{c2}(0)$ values originate from the $5d$ orbitals of M atoms, although the contribution of the $5d$ orbitals to the electronic state at E_F is small.

There are two possible mechanisms that can explain the emergence of high $H_{c2}(0)$ in Sc_6MTe_2 with $M = 5d$ elements. One is the contribution of triplet Cooper pairs in the parity-mixing superconductivity. Because Sc_6MTe_2 has a noncentrosymmetric crystal structure, triplet Cooper pairs are always hybridized with singlet pairs. The degree of this hybridization is likely to be more pronounced in the case of $5d$ elements with strong spin-orbit coupling than in the $3d$ and $4d$ cases, which might result in much higher $H_{c2}(0)$ in the $5d$ cases. The other possibility is weakening of the paramagnetic effect due to strong spin-orbit coupling, as is operative in Chevrel-phase $\text{PbMo}_6\text{S}_8^{18,19}$. In both mechanisms, strong spin-orbit coupling of M $5d$ electrons is essential, demonstrating that the characteristic features of d -electrons of M can clearly be invoked in the superconducting properties of Sc_6MTe_2 , similar to the element dependence of T_c discussed above.

In summary, the Sc_6MTe_2 series has been found to comprise unique d -electron superconductors that exhibit bulk superconductivity for all $M = 3d$, $4d$, and $5d$ elements. The critical temperature is approximately 2 K for $M = 4d$ and $5d$ elements, but higher for $M = 3d$ elements. The T_c increases in the order of $M = \text{Ni}$, Co , and Fe , and Sc_6FeTe_2 exhibits strong-coupling superconductivity with the highest T_c of 4.7 K. The upper critical field also shows a pronounced element

dependence. Sc_6MTe_2 with the $5d$ elements showed high $H_{c2}(0)$ exceeding the Pauli limit. These results clearly show that the Sc_6MTe_2 series constitutes a unique superconductor family, in which d electrons of $3d$, $4d$, and $5d$ M atoms strongly influence the superconducting properties.

Methods

Sc_6MTe_2 ($M = \text{Mn}$, Fe , Co , Ni , Ru , Rh , Os , and Ir) polycrystalline samples were synthesized by the arc melting of stoichiometric amounts of Sc chips and M and Te powders under Ar atmosphere. Sample characterization was performed by powder X-ray diffraction (XRD) with Cu $K\alpha$ radiation at room temperature using a MiniFlex diffractometer (RIGAKU). For each XRD pattern shown in Supplementary Fig. 1, all of the peaks, except for the small peaks from impurity phases including Sc_2Te , Te , and unknown impurities, could be indexed on the basis of a hexagonal unit cell with $P\bar{6}2m$ symmetry and lattice parameters almost the same as those reported in previous studies^{14,15}, indicating that the Sc_6MTe_2 with Zr_6CoAl_2 -type crystal structure was obtained as the main phase. For $M = \text{Fe}$, Co , Ru , and Ir , the obtained samples consisted of a single phase of Sc_6MTe_2 . Electrical resistivity and heat capacity measurements were performed using a Physical Property Measurement System (Quantum Design). Electrical resistivity measurements down to 0.1 K were performed using an adiabatic demagnetization refrigerator. Magnetization was measured using a Magnetic Property Measurement System (Quantum Design). First-principles calculations were performed using the WIEN2k code²⁰. Experimentally obtained structural parameters were used for the calculations^{14,15}.

Acknowledgments

The authors are grateful to R. Ishii for her support in sample preparation, T. Yamauchi for his help in magnetization measurements, and Y. Shimizu, K. Doi, H. Takei, and Z. Hiroi for helpful discussion. This work was supported by the Collaborative Research Project of Materials and Structures Laboratory, Tokyo Institute of Technology and JSPS KAKENHI (Grant Nos. 18H04314, 19H05823, and 20H02603).

References

1. J. G. Bednorz and K. A. Müller, *Zeitschrift für Physik B* **64**, 189 (1986).
2. Y. Kamihara, T. Watanabe, M. Hirano, and H. Hosono, *J. Am. Chem. Soc.* **130**, 3296 (2008).
3. F.-C. Hsu, J.-Y. Luo, K.-W. Yeh, T.-K. Chen, T.-W. Huang, Y.-C. Lee, Y.-L. Huang, Y.-Y. Chu, D.-C. Yan, and M.-K. Wu, *Proc. Natl. Acad. Sci. U.S.A.* **105**, 14262 (2008).
4. J. M. Heintz, M. Drillon, R. Küntzler, Y. Dossmann, J. P. Kappler, O. Durmeyer, and F. Gautier, *Zeitschrift für Physik B* **76**, 303 (1989).
5. Y. Maeno, H. Hashimoto, Y. Yoshida, S. Nishizaki, T. Fujita, J. G.

- Bednorz, and F. Lichtenberg, *Nature* **372**, 532 (1994).
- K. Takada, H. Sakurai, E. Takayama-Muromachi, F. Izumi, R. A. Dilanian, and T. Sasaki, *Nature* **422**, 53 (2003).
 - S. Yonezawa, Y. Muraoka, Y. Matsushita, and Z. Hiroi, *J. Phys.: Condens. Matter* **16**, L9 (2004).
 - B. R. Ortiz, S. M. L. Teicher, Y. Hu, J. L. Zuo, P. M. Sarte, E. C. Schueller, A. M. M. Abeykoon, M. J. Krogstad, S. Rosenkranz, R. Osborn, R. Seshadri, L. Balents, J. He, and S. D. Wilson, *Phys. Rev. Lett.* **125**, 247002 (2020).
 - D. Li, K. Lee, B. Y. Wang, M. Osada, S. Crossley, H. R. Lee, Y. Cui, Y. Hikita, and H. Y. Hwang, *Nature* **572**, 624 (2019).
 - H. Barz, H. C. Ku, G. P. Meisner, Z. Fisk, and B. T. Matthias, *Proc. Natl. Acad. Sci. USA* **77**, 3132 (1980).
 - G. P. Meisner, H. C. Ku, and H. Barz, *Mat. Res. Bull.* **18**, 983 (1983).
 - I. Shirovani, K. Tachi, Y. Konno, S. Kodo, and T. Yagi, *Philos. Mag. B* **79**, 767 (1999).
 - Y. Okamoto, T. Inohara, Y. Yamakawa, A. Yamakage, and K. Takenaka, *J. Phys. Soc. Jpn.* **85**, 013704 (2016).
 - P. A. Maggard and J. D. Corbett, *Inorg. Chem.* **39**, 4143 (2000).
 - L. Chen and J. D. Corbett, *Inorg. Chem.* **43**, 436 (2004).
 - K. Momma and F. Izumi, *J. Appl. Crystallogr.* **44**, 1272 (2011).
 - A. M. Clogston, *Phys. Rev. Lett.* **9**, 266 (1962).
 - Ø. Fischer, *Appl. Phys.* **16**, 1 (1978).
 - Y. Lu, T. Takayama, A. F. Bangura, Y. Katsura, D. Hashizume, and H. Takagi, *J. Phys. Soc. Jpn.* **83**, 023702 (2014).
- *E-mail: yokamoto@issp.u-tokyo.ac.jp

Supplementary Note 1. Sample characterization

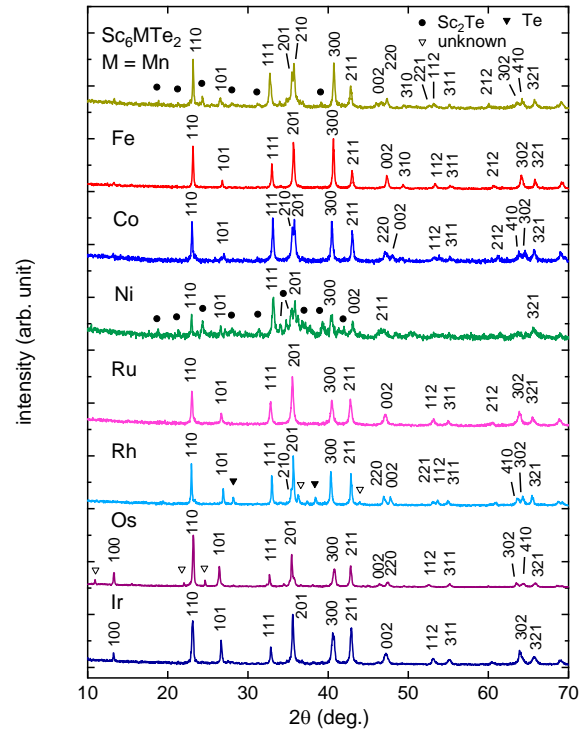
Sample characterization of Sc_6MTe_2 ($M = \text{Mn, Fe, Co, Ni, Ru, Rh, Os, and Ir}$) polycrystalline samples was performed by powder X-ray diffraction (XRD) with Cu K α radiation at room temperature using a MiniFlex diffractometer (RIGAKU). As shown in Supplementary Fig. 1, all of the peaks, except for small peaks from the impurity phases, Sc_2Te , Te, and unknown impurities, could be indexed on the basis of a hexagonal unit cell with $P\text{-}62m$ symmetry and lattice parameters almost the same as those reported in previous studies^{1,2}. This result indicated that Sc_6MTe_2 with Zr_6CoAl_2 -type crystal structure was obtained as the main phase. For $M = \text{Fe, Co, Ru, and Ir}$, the obtained samples consisted of a single phase of Sc_6MTe_2 .

References

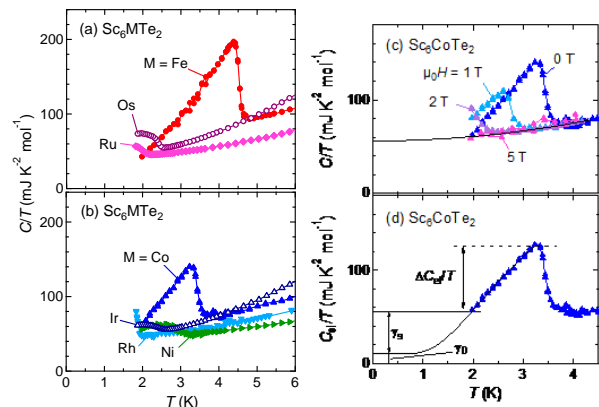
- P. A. Maggard and J. D. Corbett, *Inorg. Chem.* **39**, 4143 (2000).
- L. Chen and J. D. Corbett, *Inorg. Chem.* **43**, 436 (2004).

Supplementary Note 2. Heat capacity of Sc_6MTe_2

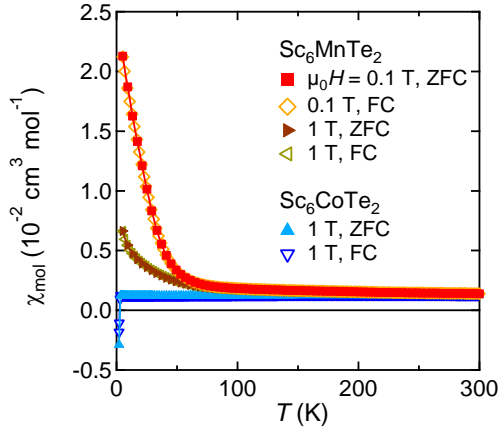
Supplementary Figs. 2(a) and (b) show the temperature dependence of heat capacity divided by temperature, C/T , for Sc_6MTe_2 ($M = \text{Fe, Co, Ni, Ru, Rh, Os, and Ir}$) polycrystalline samples. All of the data showed an anomaly corresponding to the zero-resistivity temperature, indicating the occurrence of



Supplementary Fig. 1. Powder XRD patterns of the polycrystalline samples of Sc_6MTe_2 ($M = \text{Mn, Fe, Co, Ni, Ru, Rh, Os, and Ir}$) measured at room temperature. Filled circles and filled triangles indicate the diffraction peaks of Sc_2Te and Te impurity phases, respectively. Open triangles indicate those of unknown impurities. Peak indices are given hexagonal unit cells with $P\text{-}62m$ symmetry.



Supplementary Fig. 2. (a, b) Temperature dependence of heat capacity divided by temperature, C/T , for Sc_6MTe_2 ($M = \text{Fe, Co, Ni, Ru, Rh, Os, and Ir}$) polycrystalline samples. The data for Fe, Ru, and Os are shown in (a) and those for Co, Ni, Rh, and Ir are shown in (b). (c) Temperature dependence of C/T for $M = \text{Co}$ measured at various magnetic fields. (d) Temperature dependence of electron heat capacity divided by temperature, C_{eh}/T , for $M = \text{Co}$ obtained by subtracting the lattice contribution from the data shown in (c). The broken line shows the electron heat capacity in the normal state γ .



Supplementary Fig. 3. Temperature dependences of zero-field-cooled (ZFC) and field-cooled (FC) magnetic susceptibilities of Sc_6MnTe_2 and Sc_6CoTe_2 polycrystalline samples. The data were taken at magnetic fields of 0.1 and 1 T for Sc_6MnTe_2 and at a magnetic field of 1 T for Sc_6CoTe_2 .

bulk superconductivity. The data for Fe and Co exhibited sharp jumps at T_c , while those for Os, Ir, Ni, and Ru were broad, probably reflecting the sample quality. As shown in Fig. 1(d) and Supplementary Fig. 2(c), these jumps were suppressed by applying a magnetic field, reflecting the superconducting transition. The 6.5 T data for $M = \text{Fe}$ (1.9–4.5 K) and the 5 T data for $M = \text{Co}$ (1.9–4.0 K) were fitted to the equation $C/T = AT^2 + \gamma$, yielding coefficients of the T^3 term of lattice heat capacity A of 1.07(3) and 1.19(4) $\text{mJ K}^{-4} \text{mol}^{-1}$ and Sommerfeld coefficients γ of 69.3(3) and 56.0(6) $\text{mJ K}^{-2} \text{mol}^{-1}$ for $M = \text{Fe}$ and Co , respectively.

Supplementary Fig. 2(d) shows the electron heat capacity divided by temperature, C_{el}/T , for $M = \text{Co}$ obtained by subtracting the lattice contribution from the C/T data. Similar to the Fe data shown in Fig. 1(e), the C_{el}/T data for Co are well fitted by using the sum of superconducting contributions according and the constant γ_0 , i.e. residual γ , yielding $\gamma_0 = 10 \text{ mJ K}^{-2} \text{mol}^{-1}$. The magnitude of the jump at T_c is estimated to be $\Delta C_{el}/(\gamma - \gamma_0)T_c = 1.6$ using $\Delta C_{el}/T_c = 74 \text{ mJ K}^{-2} \text{mol}^{-1}$ and $\gamma - \gamma_0 = 46 \text{ mJ K}^{-2} \text{mol}^{-1}$, which is not far from the weak-coupling limit of 1.43 for a conventional BCS superconductor. This is in contrast to the results for Fe, which showed a considerably larger jump than the weak-coupling limit value, suggesting that strong-coupling superconductivity is realized in Sc_6FeTe_2 .

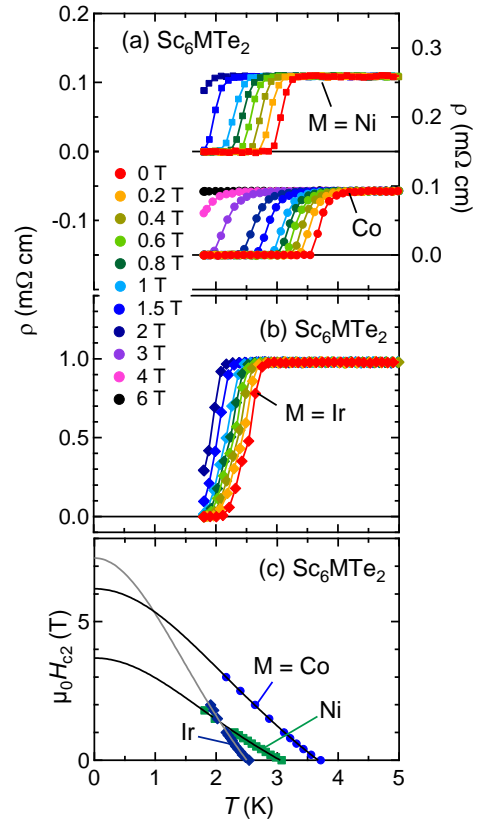
Supplementary Note 3. Magnetic susceptibility in the normal state of Sc_6MnTe_2 and Sc_6CoTe_2

As shown in Supplementary Fig. 3, magnetic susceptibility, χ_{mol} , of Sc_6CoTe_2 showed Pauli paramagnetic behavior, being almost independent of temperature. The sudden decrease of χ_{mol} at low temperature is due to the superconducting transition. In contrast, χ_{mol} of Sc_6MnTe_2 strongly increases below 50 K especially for the 0.1 T data.

Because there are no differences between the zero-field-cooled and field-cooled data, this increase is not due to magnetic long-range order, but strong magnetism, probably arising from the Mn atoms in Sc_6MnTe_2 , which might prevent Cooper pair formation therein.

Supplementary Note 4. Electrical resistivity of Sc_6MTe_2 under magnetic fields

Supplementary Figs. 4(a, b) show the electrical resistivity of Sc_6MTe_2 ($M = \text{Ni, Co, and Ir}$) measured at various magnetic fields. The upper critical field $H_{c2}(T)$ determined from the midpoint of the resistivity drop at each magnetic field for these compounds shown in Supplementary Fig. 4(c). The H_{c2} data are fitted to the Ginzburg-Landau (GL) formula $H_{c2}(T) = H_{c2}(0)[1 - (T/T_c)^2]/[1 + (T/T_c)^2]$, yielding $\mu_0 H_{c2}(0) = 3.69(2)$, $6.19(6)$, and $7.3(2)$ T and GL coherence lengths $\xi_{\text{GL}} = 9.4$, 7.3 , and 6.7 nm for $M = \text{Ni, Co, and Ir}$, respectively.



Supplementary Fig. 4. (a, b) Temperature dependences of electrical resistivity of Sc_6MTe_2 ($M = \text{Ni, Co, and Ir}$) measured at various magnetic fields. (c) Temperature dependences of the upper critical field $H_{c2}(T)$ for $M = \text{Ni, Co, and Ir}$ determined from the midpoint of the drop in the resistivity data. The solid curves show a fit to the GL formula.